Available online at www.sciencedirect.com
ScienceDirect
Ceramics International 37 (2011) 2207–2213
CERAMICS INTERNATIONAL
www.elsevier.com/locate/ceramint

Physico-chemical investigation on mixed alkali metal ferrites prepared by solution combustion method – A comparative study

B.S. Randhawa [a,*], Manik Gupta [a], H.S. Dosanjh [a], Nitendar Kumar [b]

[a] Department of Chemistry, Guru Nanak Dev University, Amritsar, Punjab 143005, India
[b] Solid State Physics Laboratory, DRDO, Timarpur, Delhi, India

Received 6 December 2010; received in revised form 10 January 2011; accepted 6 March 2011
Available online 14 April 2011

Abstract

Mixed alkali metal nanoferrites of the compositions $M_{0.5-X/2}Zn_XMn_{0.05}Fe_{2.45-X/2}O_4$ (M = Li, Na and K), where x varies from 0→0.5 in steps of 0.1, have been prepared by solution combustion method. Powder X-ray diffraction analysis for all the samples show the formation of single phase cubic spinel structure. The lattice parameter increases linearly with Zn content, which is attributed to ionic size differences of the cations involved. Both X-ray as well as experimental densities show upward trend with increasing 'x' due to increase in the molecular weight of the ferrite composition. Mössbauer spectra display the superimposition of paramagnetic doublet over ferrimagnetic sextet with increasing diamagnetic 'Zn' content. The key magnetic properties of the ferrite obtained, such as saturation magnetization and Curie temperature have also been studied. The combustion method used for the synthesis is a rapid approach for direct conversion of the stoichiometric reactant solutions into fine nanoparticles of ferrite product at a temperature (600 °C) much lower than that of the conventional ceramic method. Scanning electron micrographs confirm the formation of nanosized ferrites.

Keywords: A. Powders: chemical preparation; B. Microstructure; C. Magnetic properties; D. Ferrites

1. Introduction

The properties of the ferrite materials, which decide the application areas are generally governed by the chemical compositions and procedures followed for their preparation. Thus the chemical aspect has become the most important factor in the design and preparation of nanoferrite materials as their properties are quite different from the bulk materials. Magnetic properties are considered as the most important parameters of ferrite, as they decide the significance of the materials for any technological consideration. Some of the key magnetic properties such as saturation magnetization and Curie temperature which are generally taken into account, put a limit on the operation of frequency range and the operating temperatures respectively. Ferrites provide a wide range of properties that are useful for a variety of applications by substituting the optimum amount of various metal ions in the basic compositional formulae. Owing to the higher values of saturation magnetization and Curie temperature, substituted alkali metal ferrites find application in radar, satellite communication and microwave devices [1–8].

2. Experimental

Mixed alkali metal ferrites of the compositions $M_{0.5-X/2}Zn_XMn_{0.05}Fe_{2.45-X/2}O_4$ (M = Li, Na, K) were prepared by combustion method from stoichiometric aqueous solutions of respective metal nitrates and oxalyl dihydrazide (ODH). In these compositions 'x' varies from 0→0.5 in steps of 0.1. Stoichiometric quantities of aqueous solutions of metal nitrates and oxalyl dihydrazide were mixed and combusted in a muffle furnace at 600 °C for 2 h. The final sintering of ferrite powders compacted into disc and toroidal shapes were carried out at 1100 °C without any sintering aid. X-ray diffraction patterns were recorded for all the powder samples using Co-Kα radiation and these studies were used to calculate lattice constant 'a', densities (X-ray density and experimental density) and porosity of the ferrite samples. Magnetic parameters of

* Corresponding author.
E-mail address: balwinderrandhawa@yahoo.co.in (B.S. Randhawa).

0272-8842/$36.00
doi:10.1016/j.ceramint.2011.03.072

these samples were recorded by using vibrating sample magnetometer (VSM). ^{57}Fe Mössbauer spectra were recorded on Wissel (Germany) Mössbauer spectrometer using a ^{57}Co (Rh) γ-ray source and the velocity scale was calibrated relative to ^{57}Fe in Rh matrix. Mössbauer spectral analysis software WinNormos for Igor Pro has been used for the quantitative evaluation of the spectra. Isomer shift values are reported with respect to pure metallic iron absorber.

3. Results and discussion

3.1. X-ray studies

X-ray powder patterns of these compositions have been shown in Fig. 1 which shows formation of single spinel phase. The lattice constant '*a*' has been calculated theoretically by the following relation [9]:

$$a = \left(\frac{8}{2}\sqrt{3}\right)\left[(r_A + r_O) + \sqrt{3}(r_B + r_A)\right]$$

where r_O is the radius of oxygen ion, r_A and r_B are the ionic radii of tetrahedral (A) and octahedral (B) sites respectively. This clearly indicates that there exists a correlation between the ionic radii and the lattice constant. In order to estimate r_A and r_B in the case of more than one ion present at a site, it is necessary to know the cationic distribution of the composition. According to the thumb rule, if the radius of the substituted ion is larger than that of the displaced ion, the lattice expands and the lattice constant is expected to increase. A similar trend has been observed in the present case where the lattice constant value 'a' increases with increasing Zn substitution (Fig. 2). This can

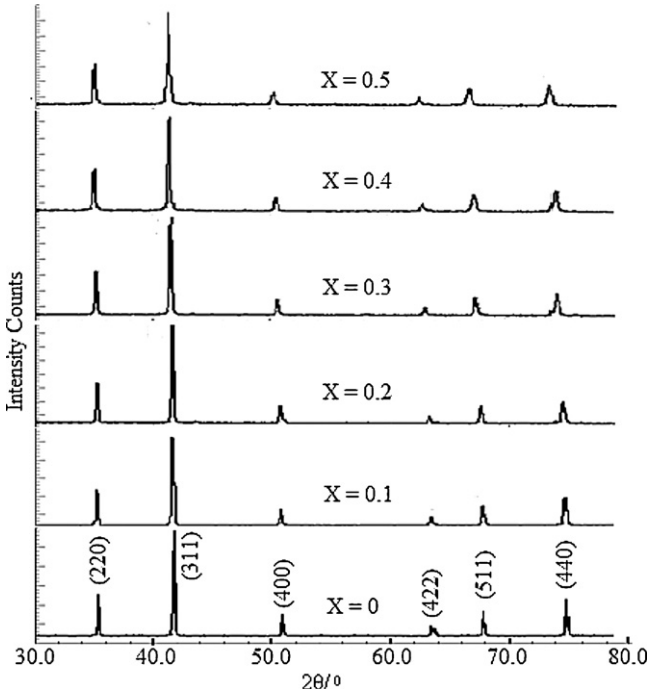

Fig. 1. X-ray powder pattern for composition $Li_{0.5-X/2}Zn_XMn_{0.05}Fe_{2.45-X/2}O_4$ with '*x*' varies from 0 to 0.5.

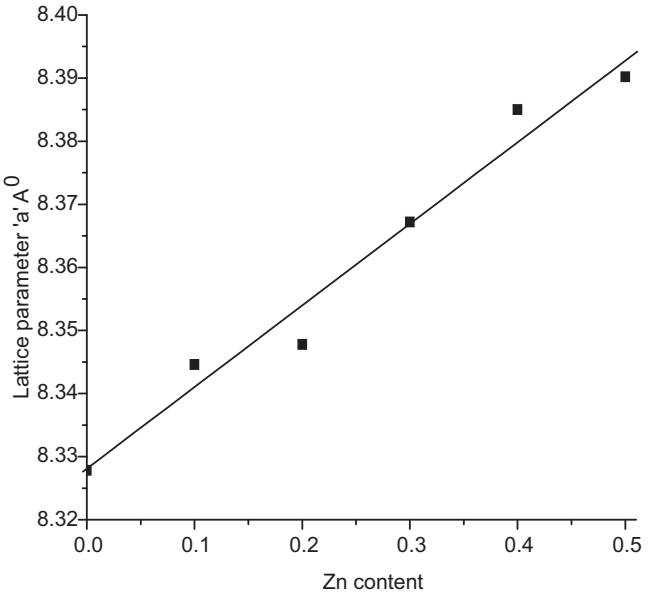

Fig. 2. Variation of lattice parameters with increasing Zn content.

be explained on the basis of volume difference between the cations, i.e. Zn^{2+} (0.083 nm), Li^+ (0.078 nm) and Fe^{3+} (0.067 nm). An increase in lattice parameter with increasing Zn content is due to the larger cationic radius of Zn^{2+} ion as compared to that of the other cations. The theoretical or X-ray density values (d_{XRD}) of various compositions of mixed lithium ferrites are listed in Table 1 and were calculated by using the relation [10],

$$d_{XRD} = \frac{8M}{Na^3}$$

where M = molecular weight of composition, N = Avogadro's number, a = lattice constant.

The theoretical density increases with the molecular mass of the composition. The experimental density or bulk density ($d_{exp.}$) has been determined for various compositions by the water immersion method [11]. Both parameters show an upward trend with increasing magnitude of '*x*'. However, the X-ray density for any given composition is higher than that of experimental density and this difference is primarily attributed to the porosity of the material. It may be mentioned that in the normal sintered ferrite it is generally not possible to control together, both porosity and grain size parameters [12–14]. The percentage porosity for all the compositions has been calculated by using the equation:

$$\left[\frac{1 - d_{exp.}}{d_{XRD}}\right] \times 100$$

The calculated values of the porosity (Table 1) have been found to be quite low which is a characteristic requirement of good quality ferrite materials, otherwise, larger magnitude of porosity deteriorates the magnetic and elastic behaviour [15] of the material even at low frequency region.

Table 1
Variation of XRD and magnetic parameters with composition 'x' for $Li_{0.5-x/2}Zn_xMn_{0.05}Fe_{2.45-x/2}O_4$.

Composition (X)	Mol. wt. (g)	d_{XRD} (g/cm^3)	$d_{exp.}$ (g/cm^3)	Lattice parameter 'a' Å	Porosity (%)	M_s (emu/g)	Curie Temp. (°C)
0	207.04	4.7614	4.5739	8.3278	3.93	30.35	634
0.1	210.44	4.8104	4.5920	8.3446	4.53	47.44	563
0.2	213.84	4.8824	4.7713	8.3478	2.27	57.19	512
0.3	217.23	4.9256	4.8109	8.3672	2.32	67.38	443
0.4	220.63	4.9709	4.8341	8.3850	3.04	58.86	360
0.5	224.03	5.0385	4.8379	8.3902	3.98	48.15	278

Table 2
Variation of XRD and magnetic parameters with composition 'x' for $Na_{0.5-x/2}Zn_xMn_{0.05}Fe_{2.45-x/2}O_4$.

Composition (X)	Mol. Wt. (g)	d_{XRD} (g/cm^3)	$d_{exp.}$(g/cm^3)	Lattice parameter 'a' (Å)	Porosity (%)	M_s (emu/g)	Curie Temp. (°C)
0	215.07	4.9802	4.7522	8.3088	4.57	1.19	397
0.1	217.66	5.0324	4.8125	8.3130	4.37	6.31	358
0.2	220.26	5.0826	4.8812	8.3184	3.96	17.18	319
0.3	222.85	5.1156	4.9145	8.3329	3.93	20.45	266
0.4	225.45	5.1732	4.9834	8.3340	3.66	9.83	217
0.5	228.05	5.2235	5.0175	8.3390	3.94	7.56	176

Table 3
Variation of XRD and magnetic parameters with composition 'x' for $K_{0.5-x/2}Zn_xMn_{0.05}Fe_{2.45-x/2}O_4$.

Composition (X)	Mol. Wt. (g)	d_{XRD} (g/cm^3)	$d_{exp.}$ (g/cm^3)	Lattice parameter 'a' (Å)	Curie Temp. (°C)	Porosity (%)	M_s (emu/g)
0	223.12	5.1802	4.7975	8.3015	267	7.39	0.50
0.1	224.91	5.2124	4.8528	8.3065	242	6.89	7.75
0.2	226.70	5.2445	4.9132	8.3114	213	6.32	9.05
0.3	228.49	5.2835	5.0672	8.3126	198	4.09	19.59
0.4	230.28	5.3205	5.1282	8.3149	175	3.61	18.12
0.5	232.07	5.3475	5.1664	8.3223	142	3.39	12.34

A similar trend for the variation of XRD parameters with increasing Zn content (x) has been observed for Na and K series (Tables 2 and 3).

Scanning electron micrographs (SEM) reveal the formation of nanosized ferrite particles (Figs. 3 and 4).

4. Magnetic studies

4.1. Saturation magnetization

Fig. 5 shows that the magnitude of saturation magnetization first increases up to a certain level of substitution and then follows the reverse trend. The saturation magnetization values for various compositions are listed in Table 1. The observed variation in the saturation magnetization can be explained on the basis of exchange interactions. The preferential site occupancy of the substituted ions in the crystallographic sublattices of the spinel structure are also taken into account for understanding the observed trend. In ferrites, Neel [16] considered three kinds of exchange interactions between unpaired electrons of magnetic ions occupying A and B sites in the crystal structure, i.e. (i) A–A interaction between magnetic ions at A-site, (ii) B–B interaction between magnetic ions at B-

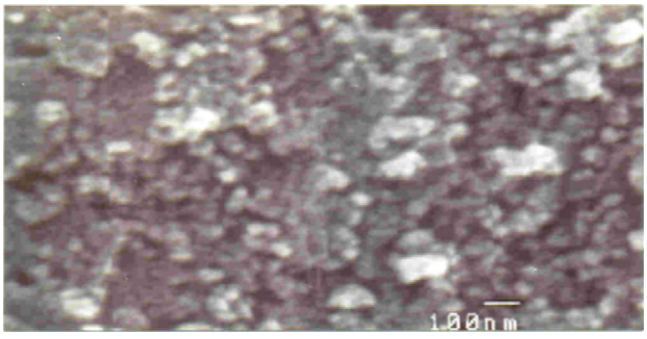

Fig. 3. SEM micrograph for composition $Li_{0.5-x/2}Zn_xMn_{0.05}Fe_{2.45-x/2}O_4$ with 'x' = 0.1.

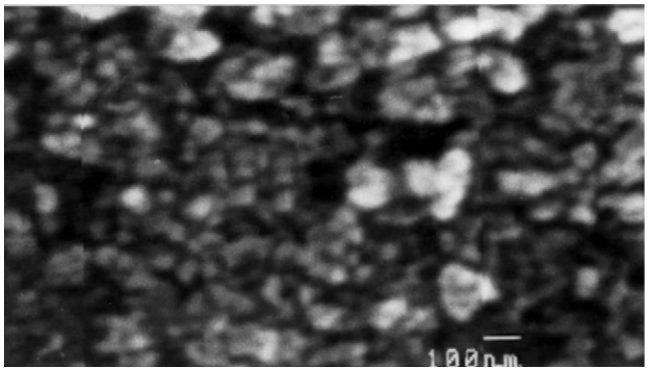

Fig. 4. SEM micrograph for composition $Li_{0.5-x/2}Zn_xMn_{0.05}Fe_{2.45-x/2}O_4$ with 'x' = 0.5.

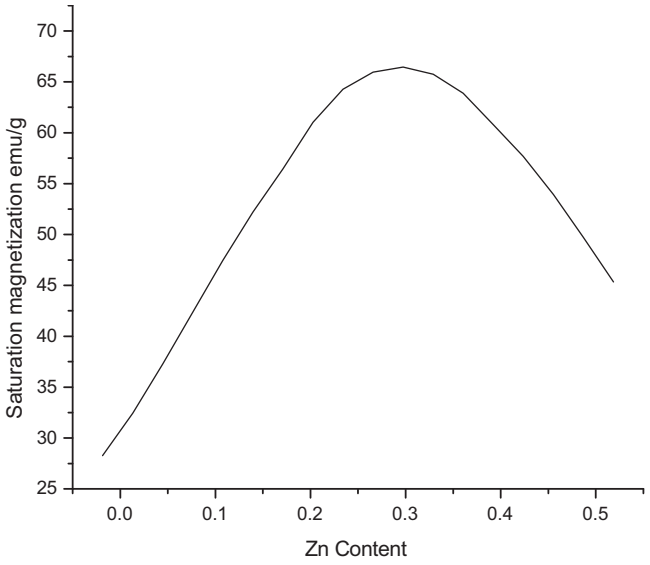

Fig. 5. Variation of saturation magnetization with increasing Zn content.

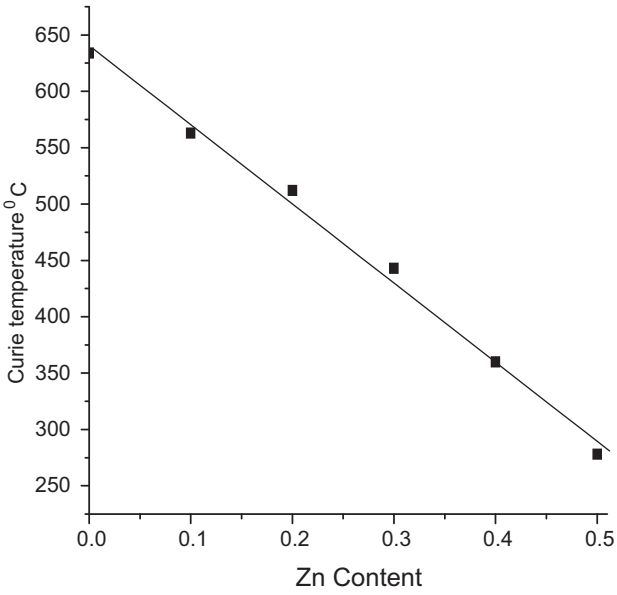

Fig. 6. Variation of Curie temperature with increasing increasing Zn content.

site, (iii) A–B interaction between magnetic ions at A and B sites.

It is known that A–B interactions are dominant as compared to A–A or B–B exchange interactions. The spins of magnetic ions are aligned by exchange interaction in tetrahedral (A) and the octahedral (B) sites in the opposite direction. As a result, the net magnetic moment (M_S) of the crystal lattice is taken as the difference between magnetic moments of B and A sublattices, i.e. $M_S = M_B – M_A$ where M_A and M_B are the net magnetic moments of ions on A and B sites. Non-magnetic Zn^{2+} ion has a strong affinity for A site and its substitution reduces the magnetization of A sublattices (M_A) and in this manner there is a net increase in the M_S value. This can be seen from experimental results where initially saturation magnetization increases with zinc ion content (x), reaches a maximum at about $x = 0.3$, and afterwards reverses its course. This phenomenon can be explained on the basis of canted spin model of Yafet and Kittel [17]. In the zinc substituted ferrite compositions, as more and more Zn^{2+} ions enter the A sublattice with increase in x, the A–B interaction naturally gets weakened. This is because of the dilution of spin moments at A site. The other interaction, i.e. B–B interaction in such a case becomes subsequently comparable to A–B interaction. In such a situation, the two sublattices will no longer be antiparallel and there will be canting of spins in B sublattice. The canting angle depends upon 'x' and a number of zinc substituted ferrites have been found to possess canted structure, whose angle of canting varies with the Zn content (x) in the system [18,19]. The observed trend for saturation

Table 4
Mössbauer parameters for various compositions of 'x' in $Na_{0.5-X/2}Zn_XMn_{0.05}Fe_{2.45-X/2}O_4$ recorded at 300 K.

Sample	[a]δ (mm/s)	Δ (mm/s)	Magnetic hyperfine field B Tesla	Distribution of Fe^{3+} ions (%)
$X = 0$	0.34	−0.005	51.09	37.56 (oct.)
	0.30	−0.001	50.67	62.44 (tet.)
$X = 0.1$	0.33	−0.004	51.06	39.53 (oct.)
	0.28	−0.002	50.56	49.17 (tet.)
	0.28	0.54	–	11.30 (C.D)
$X = 0.2$	0.33	−0.001	50.86	40.20 (oct.)
	0.29	−0.003	50.38	44.85 (tet.)
	0.30	0.58	–	14.95 (C.D.)
$X = 0.3$	0.32	−0.003	50.25	43.68 (oct.)
	0.27	0.009	41.65	40.42 (tet.)
	0.28	0.67	–	15.90 (C.D.)
$X = 0.4$	0.31	−0.002	50.18	44.55 (oct.)
	0.27	0.006	41.04	35.87 (tet.)
	0.28	0.60	–	19.58 (C.D.)
$X = 0.5$	0.31	−0.005	44.72	53.71 (oct.)
	0.26	0.009	36.27	25.51 (tet.)
	0.28	0.45	–	20.78 (C.D.)

[a] w.r.t. pure metallic iron absorber, oct. = octahedral, tet. = tetrahedral, C.D. = central doublet.

Table 5
Mössbauer parameters for various compositions of 'x' in $K_{0.5-X/2}Zn_XMn_{0.05}Fe_{2.45-X/2}O_4$ recorded at 300 K.

Sample	[a]δ (mm/s)	Δ (mm/s)	Magnetic hyperfine field B Tesla	Distribution of Fe^{3+} ions (%)
$X = 0$	0.28	−0.05	50.41	70.78 (oct.)
	0.20	−0.03	49.02	29.22 (tet.)
$X = 0.1$	0.25	−0.01	49.52	71.64 (oct.)
	0.20	−0.02	47.68	28.36 (tet.)
$X = 0.2$	0.25	0.002	48.67	70.78 (oct.)
	0.22	−0.007	46.17	27.87 (tet.)
	0.30	0.53	–	01.35 (C.D.)
$X = 0.3$	0.32	−0.004	46.15	69.26 (oct.)
	0.28	−0.007	42.38	28.85 (tet.)
	0.28	0.56	–	01.89 (C.D.)
$X = 0.4$	0.32	−0.008	45.48	68.37 (oct.)
	0.28	−0.004	40.62	27.05 (tet.)
	0.30	0.58	–	04.58 (C.D.)
$X = 0.5$	0.30	−0.004	44.72	65.57 (oct.)
	0.27	0.01	36.27	26.32 (tet.)
	0.28	0.46	–	08.11 (C.D.)

[a] w.r.t. pure metallic iron absorber, oct. = octahedral, tet. = tetrahedral, C.D. = central doublet.

magnetization value in $Li_{0.5-X/2}Zn_XMn_{0.05}Fe_{2.45-X/2}O_4$ is found to be similar to the results reported for these types of ferrites [20–23].

Mixed sodium and potassium counterparts of lithium also exhibit a similar behaviour (Tables 2 and 3).

4.2. Curie temperature

The variation in Curie temperature (T_C) with the substitution level of non-magnetic Zn^{2+} content (x) in the basic compositional formula is shown in Fig. 6. It is clear that there is a decrease in Curie temperature with increase in Zn^{2+} content (x). This variation in Curie temperature can be explained on the basis of exchange interactions. In other words, the magnitude of Curie temperature is proportional to the strength of dominant interactions, i.e. the intersublattice A–B interactions in the present case. The strength of interaction depends upon (i) the number of magnetic ions at each site, (ii) the magnetic moment of the magnetic ions, (iii) the number of interaction linkages.

A greater amount of thermal energy is required to offset the effect of exchange interaction in the material having larger number of magnetic ions and larger magnetic moments. It is well established that the replacement of a magnetic ion, Fe^{3+}, on either site of the crystal lattice by non-magnetic Zn^{2+} ions will result in the reduction of the number of magnetic linkages and consequently fall in Curie temperature [24–27]. Thus a decrease in the Curie temperature with increasing 'x' is the consequence of the substitution of non-magnetic Zn ions in the crystal lattice. As evident from Tables 2 and 3, the sodium and potassium series also show a similar trend.

4.3. Mossbauer studies

Since Mössbauer studies on mixed lithium ferrites have already been reported by us [28], therefore, Mössbauer spectra for various compositions of 'x' in $M_{0.5-X/2}Zn_XMn_{0.05}Fe_{2.45-X/2}O_4$. (M = Na, K) will only be discussed here. Mössbauer parameters recorded for sodium and potassium series are listed in Tables 4 and 5.

For mixed sodium ferrites, the observed spectrum for $x = 0$ (Fig. 7) exhibits two well resolved Zeeman sextets arising from hyperfine interactions between Fe^{3+} ions present at tetrahedral and octahedral sites (A and B sites). Mössbauer spectra for $x = 0.1$, 0.2, 0.3, 0.4 and 0.5 (Figs. 8–12) show the presence of a central paramagnetic doublet superimposed on the sextets and its intensity goes on increasing with increasing Zn^{2+} content. The central doublet may be attributed to the Fe^{3+} ions which are magnetically isolated and did not participate in long-range magnetic ordering due to a large number of nonmagnetic nearest neighbours. For diamagnetically substituted ferrites, the existence of a central

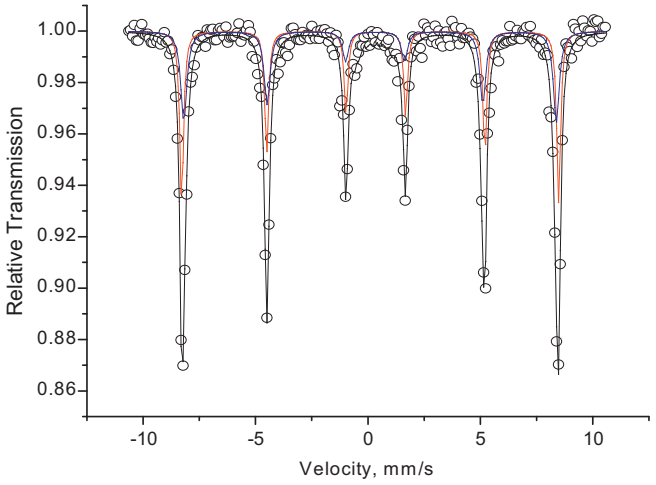

Fig. 7. Mössbauer spectrum for composition $Na_{0.5-X/2}Zn_XMn_{0.05}Fe_{2.45-X/2}O_4$ with 'x' = 0.

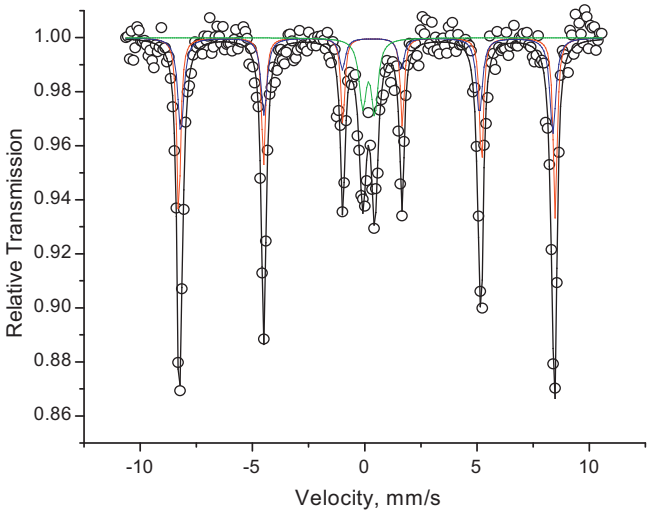

Fig. 8. Mössbauer spectrum for composition $Na_{0.5-x/2}Zn_xMn_{0.05}Fe_{2.45-x/2}O_4$ with 'x' = 0.1.

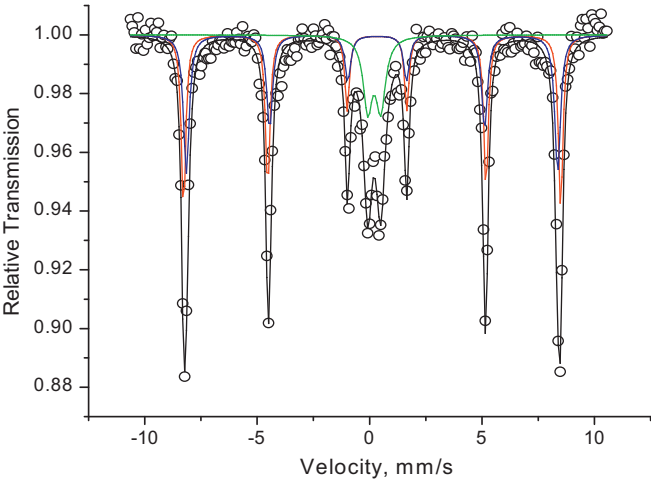

Fig. 9. Mössbauer spectrum for composition $Na_{0.5-x/2}Zn_xMn_{0.05}Fe_{2.45-x/2}O_4$ with 'x' = 0.2.

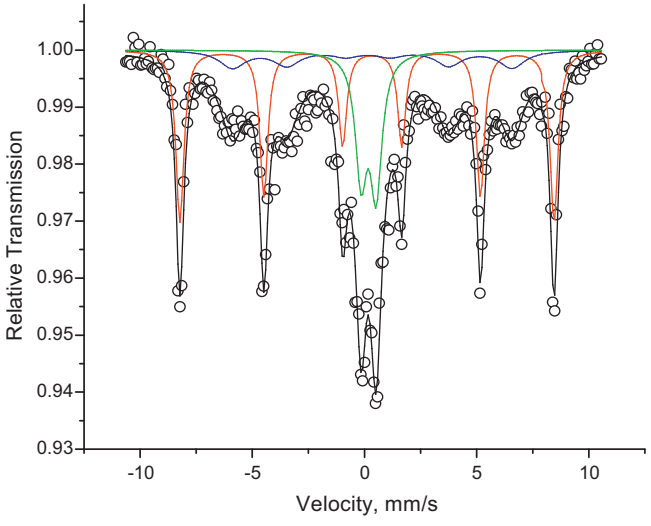

Fig. 10. Mössbauer spectrum for composition $Na_{0.5-x/2}Zn_xMn_{0.05}Fe_{2.45-x/2}O_4$ with 'x' = 0.3.

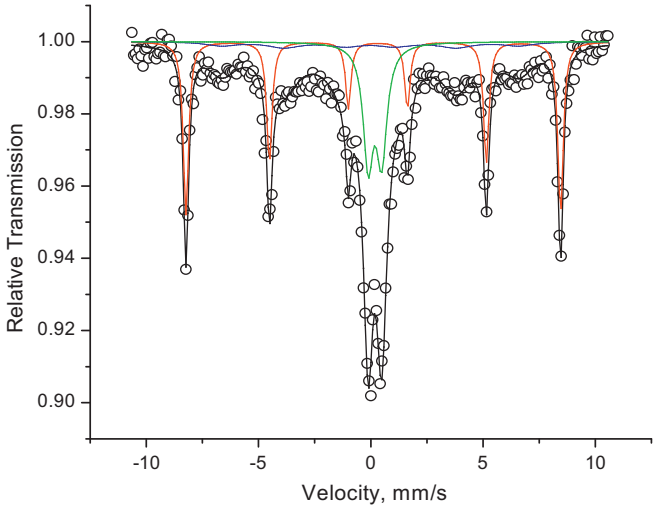

Fig. 11. Mössbauer spectrum for composition $Na_{0.5-x/2}Zn_xMn_{0.05}Fe_{2.45-x/2}O_4$ with 'x' = 0.4.

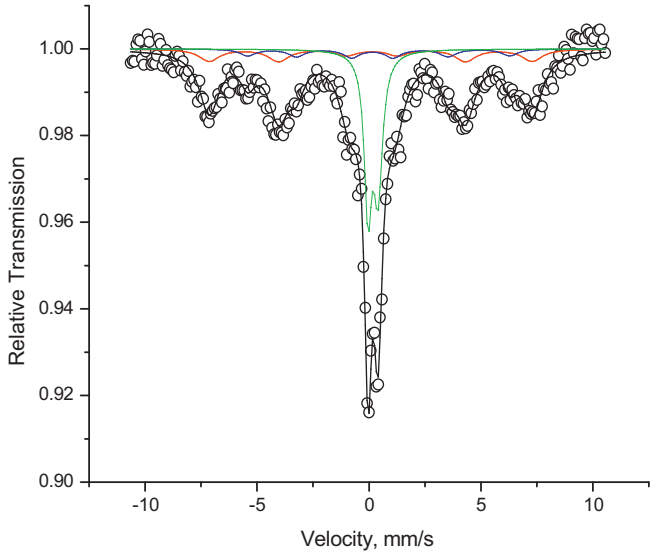

Fig. 12. Mössbauer spectrum for composition $Na_{0.5-x/2}Zn_xMn_{0.05}Fe_{2.45-x/2}O_4$ with 'x' = 0.5.

doublet superimposed on well-resolved magnetic sextets has been reported for a number of systems [29–31]. In the present system, the central doublet arises due to the magnetically isolated Fe^{3+} ions located at the tetrahedral sites and not because of any secondary phase. As expected, the isomer shift for the octahedral site is slightly greater than that of tetrahedral site (Table 4). The isomer shift values at the two sites are different because of the fact that Fe^{3+}–O^{2-} distances are different implying difference in the covalency of Fe–O bond. The Mössbauer spectra show that the magnitude of internal magnetic field at the nucleus of Fe^{3+} ions at octahedral site is higher than that of the tetrahedral site. This decrease in the hyperfine field at tetrahedral site results from the weakening of A–B exchange interaction due to the replacement of A site Fe^{3+} by non-magnetic Zn^{2+}.

Similar pattern has been displayed by mixed potassium ferrites, the Mösbauer parameters for which are summarized in Table 5.

5. Conclusions

Oxalyl dihydrazide (ODH) acts as a fuel in solution combustion method. By making use of this method, stoichiometrically pure ferrites have been obtained at lower temperature and in shorter time as compared to the conventional ceramic method. X-ray powder diffraction studies reveal the formation of single phase spinel ferrites, which ensures the high purity of materials. The lattice parameter '*a*' has been found to increase with increasing Zn content (x) which is due to the larger cationic radii of substituent Zn^{2+} ions. Mössbauer studies suggest a transition from ferrimagnetic to super-paramagnetic state with increasing diamagnetic Zn content.

In comparison, the values for saturation magnetization and Curie temperature for substituted alkali metal ferrite series show the following trend:

$$Li_{0.5-X/2}Zn_XMn_{0.05}Fe_{2.45-X/2}O_4 > Na_{0.5-X/2}Zn_XMn_{0.05}Fe_{2.45-X/2}O_4 > K_{0.5-X/2}Zn_XMn_{0.05}Fe_{2.45-X/2}O_4$$

thereby making mixed lithium ferrites the potential magnetic materials for application in radar system and microwave devices.

Acknowledgements

The authors are highly grateful to the DRDO, New Delhi for financial support.

Appendix A. Supplementary data

Supplementary data associated with this article can be found, in the online version, at doi:10.1016/j.ceramint.2011.03.072.

References

[1] J. Smit, H.P.J. Wijn, Ferrites, Tokyo Electrical Engineering College Press, Tokyo, 1965.
[2] J. Dash, S. Prasad, N. Venkataramani, P. Kishan, N. Kumar, S.D. Kulkami, S.K. Data, Study of magnetization and crystallization in sputter deposit Li–Zn ferrites thin films, J. Appl. Phys. 86 (1999) 3303.
[3] R.G. West, A.C. Blankenship, Magnetic properties of dense lithium ferrites, J. Am. Ceram. Soc. 50 (1967) 343.
[4] W. Simonet, A. Hermosin, Soft Li–Ti–Zn ferrites with resistivity $>10^8$ Ω cm, IEEE Trans. Magn. 14 (1978) 903.
[5] G.O. White, C.A. Edmondson, R.B. Goldfarb, C.E. Patton, High field magnetization studies in lithium–zinc ferrites, J. Appl. Phys. 50 (1979) 2381.
[6] F.J. Cadieu, R. Rani, W. Mendoza, B. Peng, S.A. Shaheen, M.J. Hurben, C.E. Patton, Static magnetic and microwave properties of Li-ferrite films prepared by pulsed laser deposition, J. Appl. Phys. 81 (1997) 4801.
[7] C.E. Patton, C.A. Edmondson, Y.H. Liu, Magnetic properties of lithium zinc ferrites, J. Appl. Phys. 53 (1982) 2431.
[8] D. Ravinder, Dielectric behaviour of mixed lithium–zinc ferrites, J. Mater. Sci. Lett. 11 (1992) 1498.
[9] S.A. Mazen, M.H. Abdallah, B.A. Sabrah, H.A.M. Hashem, The effect of titanium on some physical properties of $CuFe_2O_4$, Phys. Status Solidi A 134 (1992) 263.
[10] J. Smit, Ferrites: Physical Properties of Ferromagnetic Oxides in Relation to their Technical Application, Willey Interscience, New York, 1959.
[11] Annual Book of ASTM Standards, "ASTM Designation", American Society for Testing and Materials, 1971, pp. C20–C70.
[12] H. Rikukawa, Relationship between microstructures and magnetic properties of ferrites containing closed pores, IEEE Trans. Magn. 18 (1982) 1535.
[13] H. Igarashi, K. Okazaki, Effects of porosity and grain size on the magnetic properties of NiZn ferrite, J. Am. Ceram. Soc. 60 (1977) 51.
[14] V.K. Babbar, R.K. Puri, Hot-pressed Mn–Zn–Ni and Mn–Zn–Co ferrites for magnetic recording-heads, IEEE Trans. Magn. 28 (1992) 21.
[15] Y. Purushotham, V.D. Reddy, M.B. Reddy, D.R. Sager, Pran Kishan, P.V. Reddy, Elastic behaviour of titanium substituted magnesium ferrites, Mater. Res. Bull. 8 (1995) 1015.
[16] L. Neel, Magnetic properties of ferrites, ferrimagnetism and antiferromagnetism, Ann. Phys. 3 (1948) 137.
[17] Y. Yafet, C. Kittel, Antiferromagnetic arrangements in ferrites, Phys. Rev. 87 (1952) 290.
[18] N.S.S. Murthy, N.G. Natera, S.I. Youssaf, R.J. Begum, C.M. Srivastava, Yafet–Kittel angles in Zn–Ni ferrites, Phys. Rev. 181 (1969) 969.
[19] C.M. Srivastava, S.N. Shringi, R.G. Srivastava, N.G. Nanadikar, Magnetic ordering and domain wall relaxation in zinc-ferrous ferrites, Phys. Rev. B 14 (1976) 2032.
[20] E.W. Gorter, J.A. Schulkes, Reversal of spontaneous magnetization as a function of temperature in LiFeCr spinels, Phys. Rev. 89 (1953) 487.
[21] C. Guillaud, Ferrites of magnesium and zinc, Compt. Red. Acad. Sci. 232 (1951) 944.
[22] G.T. Rado, Magnetic spectra of ferrites, Rev. Mod. Phys. 25 (1953) 81.
[23] A. Vassiliev, A. Lagrange, Propriétés des ferrites de lithium partiellement substitués par l'aluminum destinés aux dispositifs micro-ondes, IEEE Trans. Magn. 2 (1966) 707.
[24] K.H. Rao, N.K. Gaur, K. Aggarwal, Effect of additives on the properties of zinc–manganese ferrite, J. Appl. Phys. 53 (1982) 1122.
[25] V. Anjali, C. Ratnamala, Effect of zinc concentration on the structural, electrical and magnetic properties of mixed Mn–Zn and Ni–Zn ferrites synthesized by the citrate precursor technique, J. Magn. Magn. Mater. 306 (2006) 313.
[26] R. Krishnan, V. Cagan, Anisotropy, magnetostriction, and In^{3+} ion distribution in nickel ferrite indate crystals, IEEE Trans. Magn. 7 (1971) 613.
[27] L.G. Van Uitert, Low magnetic saturation ferrites for microwave applications, J. Appl. Phys. 26 (1955) 1289.
[28] H.S. Dosanjh, B.S. Randhawa, Nitendar Kumar, Mössbauer effect studies on mixed lithium–zinc ferrites prepared by solution combustion method, Hyperfine Interact. 183 (2008) 45.
[29] E. De Grave, D. Chambaere, G. Robberrecht, Study of the magnetic ordering in $Fe_{1.2}Mg_{1.4}Ti_{0.4}O_4$ by means of the Mössbauer effect in external magnetic fields, J. Magn. Magn. Mater. 15 (1980) 643.
[30] E. De Grave, R. Vanleerberghe, G. Dauwe, A. Govaert, J. De Sitter, Magnetic hyperfine field distributions in ferrimagnetic spinels, J. Phys. 37 (1976) 97.
[31] K.P. Thummer, M.P. Pandya, K.H. Jani, K.B. Modi, H. Joshi, Microscopic and macroscopic magnetic properties of the $MgAl_xCr_xFe_{2-2x}O_4$ spinel ferrite system, Mater. Sci. 40 (2004) 102.